CERN-TH/99-246
NIKHEF/99-020
hep-ph/9908483

D* PRODUCTION IN TWO-PHOTON COLLISIONS

Stefano Frixione, Michael Krämer

CERN, TH Division
CH-1211 Geneva 23, Switzerland

and

Eric Laenen

NIKHEF Theory Group
Kruislaan 409, 1098SJ, Amsterdam, The Netherlands

Abstract

We calculate total and differential production rates of D^* mesons in two-photon collisions at LEP2. We include full next-to-leading order QCD corrections, and perform an extensive study of the sensitivity of our predictions to variations of the renormalization scale, charm mass, photonic parton distribution set and fragmentation function. The results are compared with recent data from LEP2.

CERN-TH/99-246
August 1999

1. INTRODUCTION

Charm quark production in two-photon collisions at high-energy e^+e^- colliders provides new possibilities to study the dynamics of heavy quark production; it complements the extensive analyses that have been carried out at fixed-target experiments and at other high-energy colliders [1]. In two-photon collisions[1] each of the photons can behave as either a point-like or a hadronic particle. Consequently, one distinguishes in such collisions direct- (both photons are point-like), single resolved- (one photon is point-like, the other hadron-like), and double resolved (both photons are hadron-like) production channels. The resolved channels require the use of parton densities in the photon, whereas the production via the direct channel is free of such phenomenological inputs. In general, the different channels mix when including higher orders in perturbation theory, and thus the distinction between the direct and resolved contributions becomes non-physical and scheme-dependent.

The mass of the heavy quark, $m_Q \gg \Lambda_{\rm QCD}$, acts as a collinear cutoff and sets the hard scale for the perturbative calculation at small heavy-quark transverse momentum p_T. It is thus possible to define an all-order infrared-safe cross section for open heavy flavour production, even at $p_T = 0$. The heavy quark mass also ensures that the separation into direct and resolved production channels is unambiguous at next-to-leading order (NLO). In the case of charm production, however, the heavy quark mass is not very large with respect to $\Lambda_{\rm QCD}$, and one therefore expects large radiative corrections in perturbative QCD. This is indeed borne out by NLO analyses of charm production in hadron–hadron and photon–hadron collisions, where the leading-order result sometimes only accounts for less than 50% of the full next-to-leading order rate [1]. As will be discussed at length in what follows, the situation in photon–photon collisions is quite different, and the predictions are under better theoretical control, in spite of the presence of resolved channels.

The OPAL collaboration has presented [2] new data for D^* production in two-photon collisions, at (mostly) $\sqrt{s_{e^+e^-}} = 189$ GeV. Besides the total cross section $\sigma^{D^*}_{\gamma\gamma}$, OPAL has measured the differential rate with respect to the D^* transverse momentum, $d\sigma^{D^*}_{\gamma\gamma}/d\,p_T^{D^*}$, and pseudorapidity $d\sigma^{D^*}_{\gamma\gamma}/d\,\eta^{D^*}$. Recently, also L3 has presented results for D^* production in two-photon collisions [3]. L3, however, does not apply an antitag condition for the scattered electrons. It is thus not obvious how the corresponding data can be compared with a theoretical calculation where the cross section is defined in the Weizsäcker–Williams approximation in the standard way.

The new LEP2 data motivated us to perform an extensive study of D^* production in two-photon collisions, including all NLO QCD corrections. We use fully differential NLO Monte Carlo programs for all the production mechanisms, constructed in refs. [4–6]. Earlier studies either focused on an individual component of the production [6], or had mostly HERA data in mind [4,5], or did not include fragmentation functions [7]. Moreover, a relatively large number of NLO-evolved photonic parton distributions [8–11], and new studies on charm fragmentation functions [12–14] are available, some of them incorporating the most recent theoretical and experimental findings. We shall examine in detail the sensitivity of the NLO

[1] In this paper, we will only consider the case in which the incoming photons are on-shell.

calculations of D^* meson cross sections with respect to variations of the renormalization scale, charm mass, photonic parton distribution sets, fragmentation function, and others.

The paper is organized as follows. In section 2 we review very briefly the NLO Monte Carlo programs that we used in the rest of the paper. The results of our study, and the comparison of our calculations with the OPAL data, are presented in section 3. We summarize our work in section 4. The computation of photon–photon cross sections and the issue of scheme dependence of the direct and resolved production mechanisms is discussed in the appendix.

2. NLO MONTE CARLO PROGRAMS

We consider the process

$$e^+ + e^- \longrightarrow e^+ + e^- + Q + \overline{Q}, \tag{1}$$

where the final state positron and electron are scattered almost collinearly to the beam line. The cross section is dominated by the scattering of two on-shell photons, which produce the heavy quarks and can be written as a convolution of two Weizsäcker–Williams spectra [15] with the cross section for the process $\gamma\gamma \to Q\overline{Q}$. As mentioned in the introduction, besides the direct contribution, also resolved production channels have to be taken into account. The cross section for the resolved contributions factorizes into a partonic hard-scattering cross section, convoluted with photonic light-quark and gluon densities. Notice that these densities grow as $\alpha_{\rm em}/\alpha_S$ at large scales, owing to the inhomogeneous term in the relevant Altarelli–Parisi equations; therefore, the cross sections for the resolved processes are formally of the same perturbative order as the cross section for the direct process. More details on the computation of photon–photon rates in perturbative QCD will be given in the appendix.

To calculate the direct and resolved contributions including the complete NLO corrections, we use Monte Carlo programs that are fully exclusive in all final-state particles. We want to emphasize that our programs are different from the usual Monte-Carlo parton-shower codes, since they result from fixed-order QCD computations, where no collinear approximation (and no shower evolution) has been performed. For the direct channel, the NLO program has been constructed in [6], while for the single-resolved and double-resolved channels we use the NLO programs constructed in refs. [4,5]. To check our results we employed in addition the single-particle inclusive programs of refs. [7,16,17]. In our codes all final-state kinematical quantities are available on an event-by-event basis, and it is thus possible to calculate any infrared-safe quantity to NLO, if the quantity requires two or three partons for its definition, or to LO if it requires three partons, with any final-state kinematical cuts matching those implemented by experiments. This allows us to compare NLO predictions with measurements in the experimentally visible region. As will be discussed below, cross section extrapolation beyond the accepted region introduces large theoretical uncertainties, at least for the case at hand, and we find the visible cross section to be as important as the total cross section for the comparison of data with theory. The wide avail-

ability of flexible higher order Monte Carlo programs in which acceptance cuts can be easily built in makes the calculation of many types of visible cross section practical, thereby providing the possibility of a more detailed comparison between theoretical and experimental results at high energy colliders.

3. RESULTS

We will first define a default set of input parameters and then study parameter variations to examine the sensitivity of our theoretical predictions. The collision energy is fixed at $\sqrt{s_{e^+e^-}} = 189$ GeV. We set the charm quark mass, defined in the on-shell renormalization scheme, to $m_c = 1.5$ GeV. The two-loop expression for the QCD coupling is used, with $\Lambda^{(5)}_{\overline{\rm MS}} = 220$ MeV, as favoured by recent global QCD fits. The default choice for the renormalization scale is $\mu_R^2 = m_T^2 \equiv m_c^2 + p_T(c)^2$, and for the factorization scale we use $\mu_F^2 = 4m_T^2$. Our default choice for the photonic parton densities entering the resolved channels is the recent NLO-evolved set GRS-HO [11]. We checked that, by adopting the GRS-HO set defined in the $\overline{\rm MS}$ or DIS$_\gamma$ [18] scheme, and changing the short-distance cross sections accordingly, only numerically negligible differences arise. Finally, for the Weizsäcker–Williams function we adopt the form proposed in ref. [19], designed to describe an antitag condition on the scattered electron. Here, the antitag angle is $\theta_{\rm max} = 0.033$, as determined by the OPAL experimental setup. The Peterson et al. parametrization [20] is used as the charm-to-D^* fragmentation function, normalized according to $\int_0^1 dz D(z,\epsilon) = 1$. Our default value for the non-perturbative parameter entering the fragmentation function will be $\epsilon = 0.035$ (see for example ref. [14]). In order to obtain the D^* kinematical variables from those of the fragmenting charm quark, we rescale the three space components of the parton momentum with the momentum fraction z, and compute the energy according to the charm quark mass shell condition (the choice of mass to fix the D^* energy component is arbitrary, because the factorization theorem only holds for large p_T, where mass effects are negligible. We have checked that our numerical results in the experimentally visible region $p_T(D^*) \gtrsim 2$ GeV are not sensitive to the specific choice).

We have to comment on the fact that the $\Lambda_{\rm QCD}$ value we use is not the one associated with the GRS-HO photon set. The parton densities are correlated with $\Lambda_{\rm QCD}$ [2], so that, in principle, $\Lambda_{\rm QCD}$ cannot be chosen independently of the PDF set. However, in practice, it is known that the correlation between $\Lambda_{\rm QCD}$ and the densities of the photon is very mild [21], and our choice can be considered safe, also given the fact that other theoretical uncertainties are dominant in charm physics. Since our aim is to compare theory with experimental data and because the normalization of the resolved contributions is very sensitive to the choice of $\Lambda_{\rm QCD}$, we deem it appropriate to use an up-to-date value for $\Lambda_{\rm QCD}$. As a final comment on our default choices, we remark that we prefer to use $\mu_F = 2m_T$ rather than $\mu_F = m_T$ as the factorization scale: at very low transverse momenta, $\mu_F = m_T$ would probe the parton densities at a scale where the validity of the evolution equations is not on firm grounds. As

[2] The correlation is due to the Altarelli–Parisi evolution equation, and to the fact that the largest sensitivity is to $\alpha_S g(x)$, where $g(x)$ is the gluon density, and not to $g(x)$.

is customary in charm physics, we will not consider the variation of our results with respect to μ_F, for the same reason. The scale uncertainty that we will quote therefore only partially accounts for the full theoretical error.

3.1. TOTAL CROSS SECTIONS

The preliminary value obtained by OPAL for the total cross section for D^* production in $\gamma\gamma$ collisions at $\sqrt{s_{e^+e^-}} = 189$ GeV, in the range $2 < p_T(D^*) < 12$ GeV and with the cut $|\eta(D^*)| < 1.5$ is

$$\sigma(e^+e^- \to e^+e^- D^* X)_{[2<p_T(D^*)<12 \text{ GeV};|\eta(D^*)|<1.5]} = 29.9 \pm 4.2 \text{ pb} \quad \text{(OPAL)}. \tag{2}$$

Taking into account the probability for a charm quark to fragment into a D^* meson (we use here $f(c \to D^{*+}) = 0.233 \pm 0.010$, the same value as adopted in ref. [2]), and the fact that OPAL counts both the heavy quark and the heavy antiquark in their cross-section determination, we find a theoretical value of

$$\sigma(e^+e^- \to e^+e^- D^* X)_{[2<p_T(D^*)<12 \text{ GeV};|\eta(D^*)|<1.5]} = 17.3\ ^{+5.1}_{-2.9} \text{ pb} \quad \text{(NLO QCD)}. \tag{3}$$

The theoretical error reflects the dependence on the charm quark mass, chosen in the range $1.2 \le m_c \le 1.8$ GeV, and the renormalization scale uncertainty, $m_T/2 \le \mu_R \le 2m_T$. The renormalization scale has been varied independently for the direct and resolved contributions. We observe that the central NLO prediction underestimates the experimental data, which seems to suggest that the input parameters should be taken such as to yield the largest possible cross section. This issue will be discussed in more detail in the next subsection.

To provide more detailed information on the NLO QCD cross section prediction and on the theoretical uncertainties, we have collected the results for the total and the visible cross section in table 1, including the variation of different input parameters. We consider the effect of changing the renormalization scale and the charm quark mass, and of adopting the photon density sets GRV-HO [8] and AFG-HO [9]. We also show the sensitivity to $\Lambda_{\rm QCD}$ by choosing $\Lambda^{(4)}_{\overline{\rm MS}} = 200$ MeV, which is equal to the value associated with GRV-HO and is smaller than that associated with GRS-HO. The first two columns of the table present total cross sections in the full phase space (i.e. no final-state kinematical cuts are applied); they differ in the choice of the reference scale μ_0, which in the first column is set to a fixed value (the charm mass), while in the second column it depends on the final-state kinematics (the scale is set equal to the transverse mass). Since the total cross section is dominated by small transverse momenta, $p_T \simeq m_c$, the difference between choosing a fixed or a p_T-dependent scale is less than about 10% for the sum of direct and resolved contributions. Finally, the third column displays the predictions for the visible range, defined by the OPAL cuts. It is obvious from table 1 that the visible cross section is much more stable under scale and mass variations than the fully extrapolated one and thus provides an important and in certain aspects better quantity for comparison of data with theory. The dependence of the theoretical uncertainties upon the kinematical cuts will also be studied in the following.

$\sigma_{D\bar{D}^*}$ (pb)		$\mu_0 = m_c$	$\mu_0 = m_T$	$\mu_0 = m_T$ $2 < p_T < 12$ GeV $\lvert\eta\rvert < 1.5$; $\epsilon = 0.035$
Total	Default	871.1	827.8	37.22
	$\mu_R = 2\mu_0$	742.2	727.1	35.46
	$\mu_R = \mu_0/2$	1204	1035	40.45
	$m_c = 1.2$ GeV	1712	1591	41.70
	$m_c = 1.8$ GeV	504.8	485.6	32.7
	$\Lambda^{(4)} = 200$ MeV	751.2	733.0	35.35
	GRV-HO	1053	984.6	42.14
	AFG-HO	906.4	856.2	39.74
Direct	Default	590.5	577.5	26.20
	$\mu_R = 2\mu_0$	528.9	522.8	26.60
	$\mu_R = \mu_0/2$	772.7	723.0	25.57
	$m_c = 1.2$ GeV	1098	1066	27.79
	$m_c = 1.8$ GeV	357.3	350.9	24.10
	$\Lambda^{(4)} = 200$ MeV	546.0	538.4	26.46
Resolved	Default	280.6	250.3	11.02
	$\mu_R = 2\mu_0$	213.3	204.3	8.860
	$\mu_R = \mu_0/2$	430.8	311.5	14.88
	$m_c = 1.2$ GeV	613.9	524.5	13.91
	$m_c = 1.8$ GeV	147.5	134.7	8.659
	$\Lambda^{(4)} = 200$ MeV	205.2	194.6	8.894
	GRV-HO	462.6	407.1	15.94
	AFG-HO	315.9	278.7	13.54

Table 1: *Results for the total cross section broken down to the direct and the (single- plus double-) resolved photon contributions. The results in the first two columns are independent of the value of ϵ. The factorization scale is $\mu_F = 2\mu_0$. The renormalization scale is $\mu_R = \mu_0$, unless otherwise indicated. Note that the fragmentation function is normalized according to $\int_0^1 dz D(z,\epsilon) = 1$ as described in the text.*

3.2. DIFFERENTIAL DISTRIBUTIONS

The study of differential distributions constitutes a more comprehensive test of the theory than that of total cross sections alone. In this section we concentrate on the single-inclusive distributions in transverse momentum p_T and pseudorapidity η, for which experimental data are now available. We emphasize that with our Monte Carlo programs also more exclusive observables can be calculated at NLO, so that additional comparisons can be made, should experimental data become available in the future. In the following, we have defined the Born cross section for the resolved channels as the lowest-order partonic cross sections computed with two-loop α_S and convoluted with NLO-evolved photonic parton density sets. This choice implies that the difference between the Born and NLO results is essentially due to the short-distance parton dynamics, as is the case of the direct part.

In fig. 1 we show our predictions for the p_T and η distributions using the default set of parameters. The cuts $|\eta(D^*)| < 1.5$ and $2 < p_T(D^*) < 15$ GeV have been applied, respectively. The total cross sections are decomposed into the direct, single-resolved and double-resolved components. We stress again that these quantities are not physical in general, although at this order the direct component is well defined as such. The relative size of the single- and double-resolved components is factorization-scheme- and scale-dependent; however, for both the $\overline{\rm MS}$ and DIS$_\gamma$ schemes, and regardless of the specific choice for μ_F, the double-resolved component contributes only very marginally to the charm cross section at LEP2 energies. The direct channel dominates the cross section in the visible range, even more so for large p_T. As for the η distribution, one observes that the direct channel dominates at central values, but that the single-resolved contribution extends further out in pseudorapidity. Therefore, when only large values of η are considered, there is an enhanced sensitivity to resolved contributions, making it in principle a good observable for learning about the partonic densities [3]. However, in practice it is very hard for the LEP experiments to properly identify charmed mesons in such forward regions. Therefore, we shall not pursue the study of such observables here.

Let us briefly comment on the effects of resumming large logarithms $\log(p_T/m_c)$, which arise beyond LO from the collinear emission of gluons by heavy quarks at large p_T, or from almost collinear branching of gluons into charm-quark pairs. At $p_T \gg m_c$ these terms might spoil the convergence of the perturbation series and lead to large scale dependences of the NLO result. The large logarithms can be resummed by neglecting in the matrix elements all the power-suppressed mass terms (which behave like m_c/p_T to some power; this is the reason why this approach is often – not very rigorously – denoted as "massless"), and absorbing the mass singularities, occurring as powers of $\log(p_T/m_c)$, into parton distribution functions and parton-to-heavy-quark fragmentation functions. The fragmentation functions can be computed in perturbation theory [22] at a scale of the order of the heavy quark mass, and subsequently evolved to the appropriate scale (which is of the order of p_T) by using the Altarelli–Parisi equations; in this evolution, large logarithms are properly resummed. A study of such a resummation in photon–photon collisions has been presented in ref. [23].

[3] Similar observables for inclusive jet final states at the Tevatron are indeed used for such purposes.

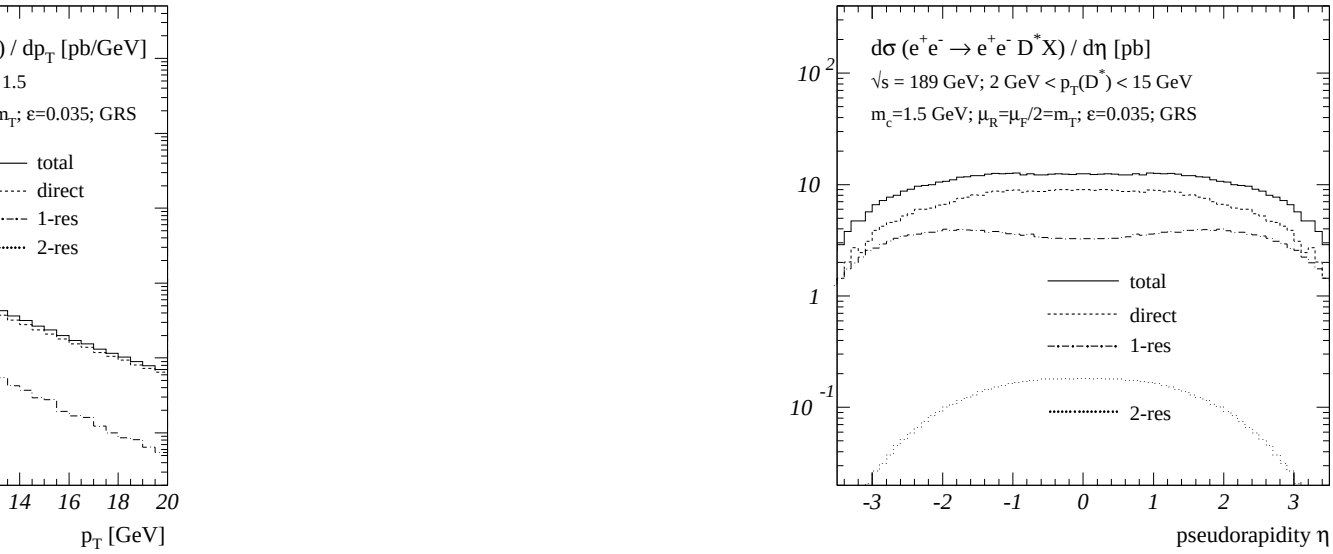

Figure 1: *NLO predictions for the D^* transverse momentum and pseudorapidity distributions, with default parameters (solid line). The direct, single-resolved (1-res) and double-resolved (2-res) results are also shown.*

We would like to emphasize that the resummed calculation is not reliable unless $p_T \gg m_c$, since all non-singular mass terms are neglected. We have verified numerically that omitting those mass terms from the NLO cross section overestimates the full result by no less than $\approx 100\%$ at $m_c/p_T \approx 1$ and still by $\approx 25\%$ at $m_c/p_T \approx 1/4$. The observation of ref. [23], that resummed and fixed-order calculation agree down to relatively small values of p_T, must therefore be considered accidental. Similar findings have been made in an analysis of the p_T spectrum in heavy-flavour hadroproduction [24]. We conclude that a comparison of the photon–photon D^* data and the resummed approach is not meaningful unless $p_T(c) \gtrsim$ 6–7 GeV.

The relative contribution of the direct, single- and double-resolved components to the differential cross section is displayed in fig. 2 as a function of p_T and η. The curves are shown for both Born and NLO cross sections. In most of the p_T range the relative fractions at the Born and NLO level are rather similar, even more so for large p_T, since the value of $\alpha_S(m_T)$ is decreasing with increasing transverse momentum. On the other hand, the relative fraction changes sizeably over the whole range of η when radiative corrections are included, because the visible cross section is dominated by the region of low $p_T \gtrsim 2$ GeV. In general, the radiative corrections tend to increase the importance of the resolved processes. Although the relative contribution of the resolved cross section never exceeds 30% (with the default set of parameters), NNLO corrections may increase the importance of the resolved channels and thereby enhance the total D^* cross section. The NLO single-resolved fraction falls below the LO value at low $p_T \lesssim 1$ GeV, causing the NLO direct fraction to exceed the LO one. This is due to the γq subprocess in the single-resolved component, which is only

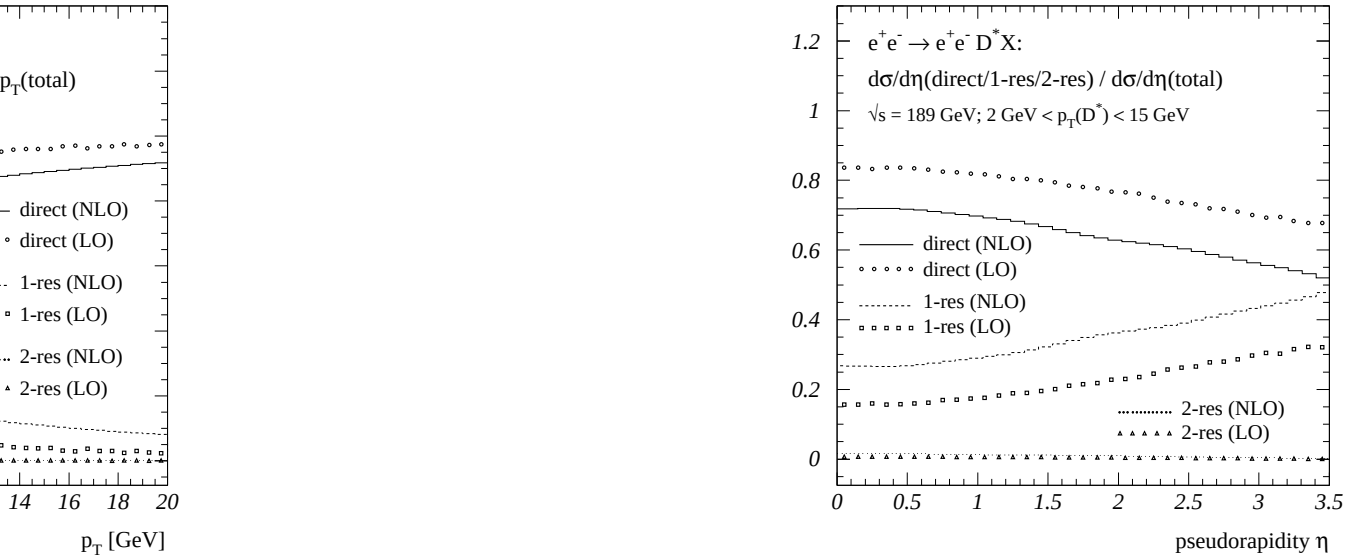

Figure 2: *Relative contributions of the direct, single-resolved and double-resolved processes to the total cross section, as a function of transverse momentum and pseudorapidity. Both the NLO (histograms) and Born (symbols) results are presented. Default parameters as specified in the text.*

present from NLO onwards and which gives a negative contribution at low p_T. The same behaviour turns out to occur for the double-resolved component, where the qg-initiated subprocess decreases the NLO cross section at very small p_T.

In fig. 3 we show the ratio of the NLO cross section over the Born cross section (K-factor), as a function of p_T and η. The K-factor is decreasing with increasing transverse momentum, a consequence of the decreasing $\alpha_S(m_T)$ and the increasing relative size of the direct contribution. In the visible range $2 < p_T < 15$ GeV the K-factor is moderate, ranging approximately from 1.2 to 0.75. This has to be compared with the case of photon–hadron and hadron–hadron collisions, where much larger K-factors (up to $K \sim 2$) are observed and where NNLO corrections are expected to be sizeable. The dependence of the K-factor on the pseudorapidity η, also shown in 3, is very mild.

Let us now turn to the sensitivity of the transverse momentum distribution to variations of the input parameters. Figure. 4 shows the p_T spectrum of the D^* for different choices for the renormalization scale, the charm quark mass, the NLO photonic parton density set, and the shape of the Peterson et al. fragmentation function as controlled by the parameter ϵ. The scale, mass and parton density dependence is sizeable at small $p_T \lesssim 2$ GeV, the biggest uncertainty coming from the variation of the charm quark mass. The strong renormalization scale and charm mass dependence is mainly induced by the large variation in the value of $\alpha_S(m_T)$. For the lowest charm quark mass value considered, and at small p_T, the hard scale of the process, $m_T \sim 1.5$ GeV, may indeed be too small to allow for a reliable perturbative analysis. However, the situation is much improved in the region probed by experiment,

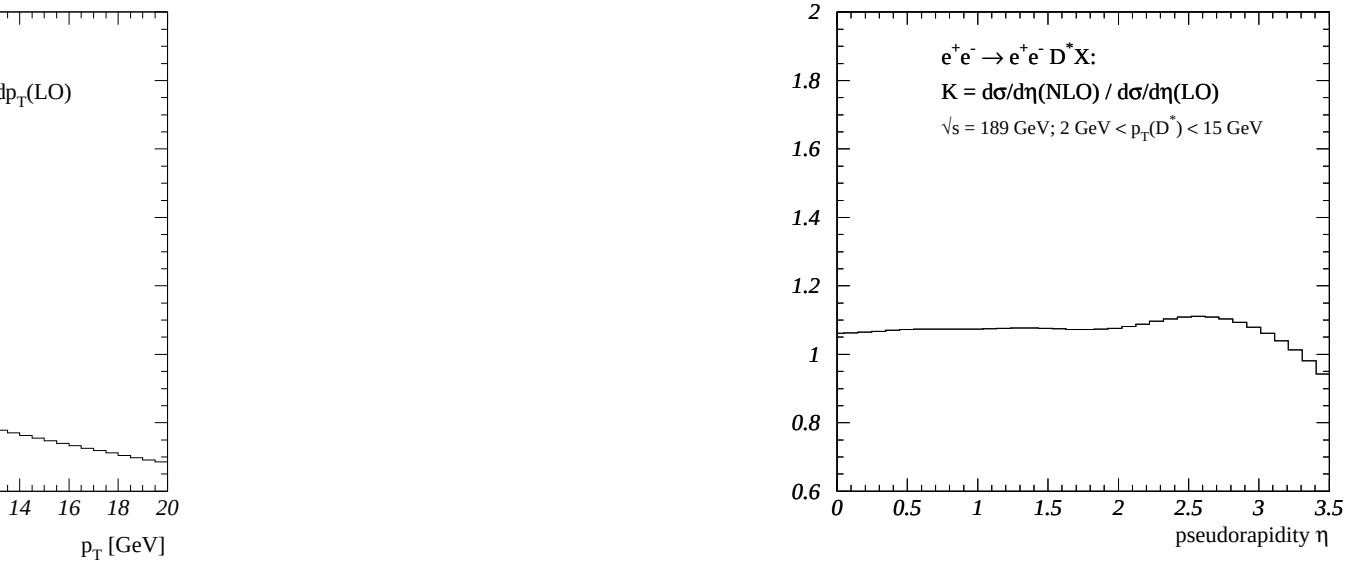

Figure 3: *Ratio of NLO over Born result, as a function of transverse momentum and pseudorapidity. Default parameters as specified in the text.*

$p_T \gtrsim 2$ GeV, where the scale and mass dependence is modest and the theoretical predictions appears to be well under control. The reduced theoretical uncertainty is a consequence both of the increase of the hard scale and of the increasing importance of the direct contribution, which receives only small radiative corrections above $p_T \gtrsim 2$ GeV. This fact, together with the behaviour of the K-factor previously discussed, leads us to the conclusion that charm production in photon–photon collisions is under better theoretical control than in photon–hadron or hadron–hadron collisions.

The dependence upon the parton density sets is mild and visible in the low-p_T region only, where the resolved contribution is still sizeable (this is also illustrated in table 1). The average Bjorken-x probed is of the order of $2m_T/\sqrt{s_{\gamma\gamma}}$, so that the photonic parton densities can in principle be tested in a region where they are poorly constrained by available data. Unfortunately, the sizeable theoretical uncertainty due to other sources in the cross section prediction at small p_T prevents a discrimination of the different PDF sets.

Finally, in the last plot of fig. 4 we show the sensitivity of the p_T spectrum to the shape of the fragmentation function by varying the ϵ parameter that enters the Peterson et al. form. We have considered, together with our default value $\epsilon = 0.035$, the more extreme choice $\epsilon = 0.02$, as obtained in recent fits [14] where the resummation of large collinear logarithms is taken into account. We remind the reader that the ϵ values obtained from older fits [25] were significantly higher ($\epsilon \sim 0.06$), resulting in a softer p_T spectrum. There seems to be a clear indication now that the degradation of the momentum of the parent charm quark should be smaller (the very same effect is also emerging in b physics). We also display the purely perturbative result without fragmentation, corresponding to $\epsilon = 0$.

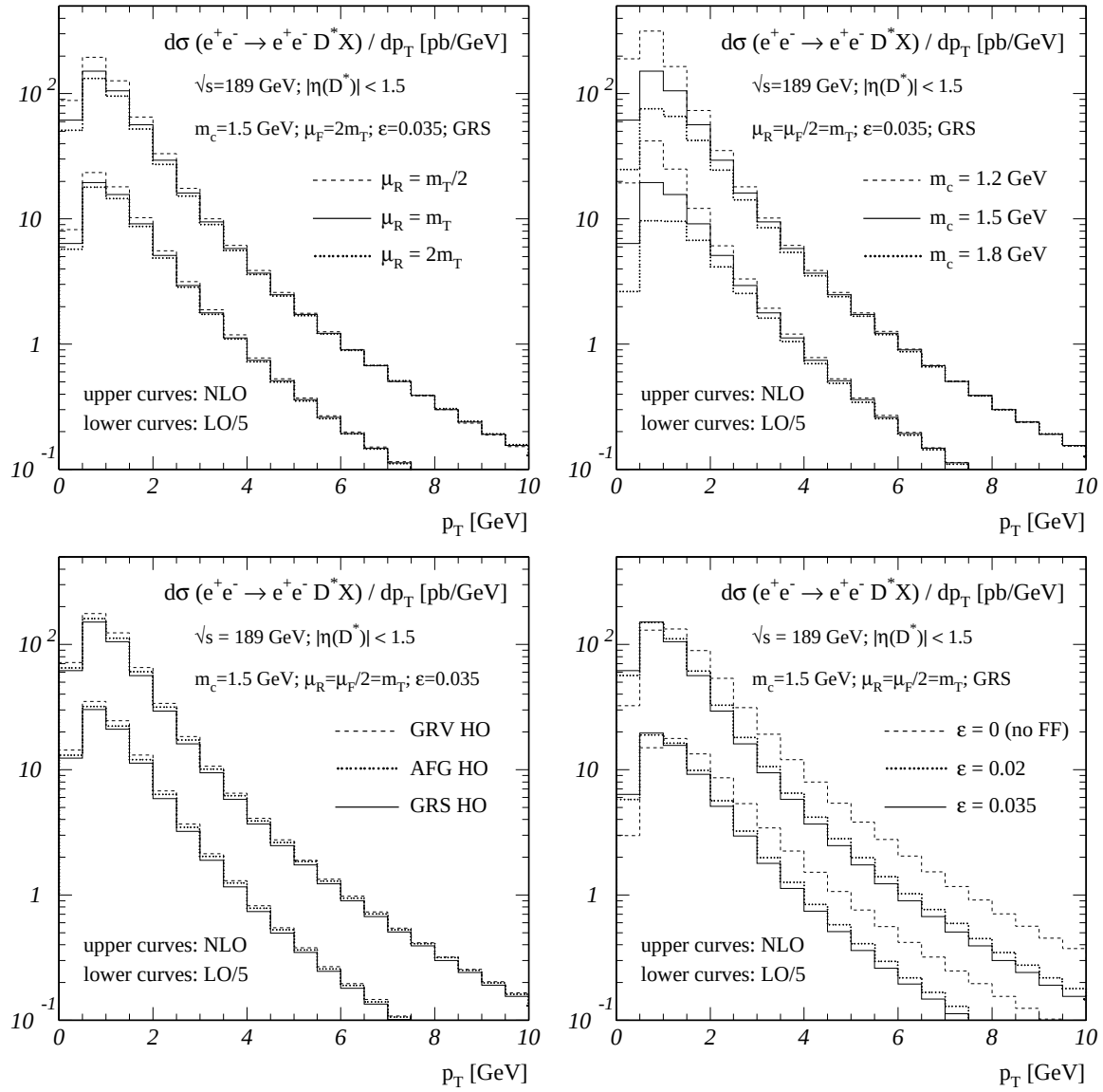

Figure 4: *Dependence of the p_T spectrum of the D^* upon renormalization scale, charm mass, photonic parton densities and the parameter ϵ of the Peterson et al. fragmentation function. Both the NLO (upper curves) and the LO (rescaled by 1/5; lower curves) results are presented.*

From the figure one can conclude that the p_T spectrum of the D^* in $\gamma\gamma$ collisions is not sensitive enough to the value of ϵ to discriminate between $\epsilon = 0.035$ and $\epsilon = 0.02$. On the other hand, the purely perturbative prediction without fragmentation function results in a much harder spectrum, which, as will be shown later in this section, is not favoured by the experimental data. Let us mention that the need to include a fragmentation function is not always obvious from a comparison with data; measurements of B meson production

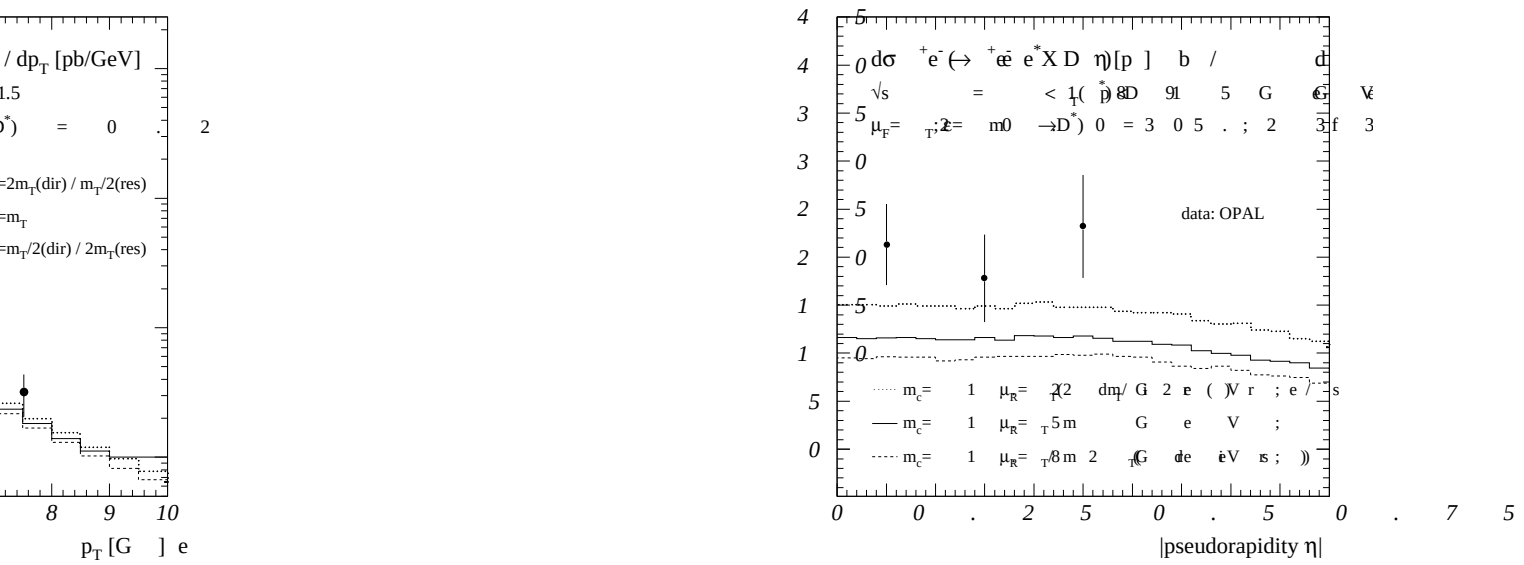

Figure 5: *Comparison between the NLO theoretical prediction and the OPAL data. The theoretical band is obtained by varying both the renormalization scale and the charm mass. The theoretical curves include the probability for a charm quark to fragment into a D^* meson $f(c \to D^{*+}) = 0.233$ and take into account the fact that OPAL counts both the heavy quark and the heavy antiquark in their cross-section determination.*

in $p\bar{p}$ collisions at the Tevatron are consistent with a purely perturbative prediction, thus (provocatively) suggesting $\epsilon = 0$.

The detailed studies of charm production at fixed-target experiments imply the relevance of non-perturbative effects, such as the intrinsic transverse momentum of the incoming partons [1]. We attempted to model such effects by supplying the initial-state partons with a Gaussian-distributed transverse momentum. Although such a procedure is not fully consistent when radiative corrections are included, it can nevertheless provide an estimate of the relevance of these non-perturbative phenomena. We have studied this issue also in the case of photon–photon collisions and find that intrinsic transverse momentum effects are completely negligible, even if the average transverse momentum of the partons is chosen as large as 2 to 3 GeV.

In fig. 5 we finally compare our predictions for the D^* transverse momentum and pseudorapidity distribution with the OPAL measurement. Three different theoretical curves are shown, where the charm quark mass and the renormalization scale are varied as indicated in the figure, while the photonic parton density and charm-to-D^* fragmentation function are kept fixed at the default choice. The theoretical results include the probability for a charm quark to fragment into a D^* meson $f(c \to D^{*+}) = 0.233$ and take into account the fact that OPAL counts both the heavy quark and the heavy antiquark in their cross-section determination. We can conclude that the data agree reasonably well with the NLO pre-

dictions. More specifically, we can see that the shape of the distributions is reproduced quite well, while there is a small discrepancy in absolute normalization, of the same size as that observed when discussing the total rates. Of course, a definite conclusion will only be possible after the statistical errors affecting the data will decrease; at present, the data seem to suggest that the input parameters should be taken such as to yield the largest possible cross section. However, it is difficult to disentangle the various effects that could play a rôle here. We could indeed enlarge the cross section by taking a small mass value, a small renormalization scale, photonic densities with much softer gluon, or a combination of these three effects. Furthermore, the inclusion of NNLO is expected to further increase our prediction. In general, we can observe that theory undershoots the data when central values for the input parameters are adopted, as is the case for many such comparisons for charm production at various colliders.

4. SUMMARY

We have performed a full NLO QCD study of total and differential D^* production rates in two-photon collisions at LEP2. Compared with charmed-meson production in hadron–hadron or photon–hadron collisions, the two-photon cross section appears to be under better theoretical control, mainly because of the dominance of the direct channel, where QCD corrections are smaller than in the case of the resolved channels. This consideration holds in particular for the moderate- and high-p_T region and for the central η region, which are directly probed by LEP experiments. We find the largest theoretical uncertainties, due to charm mass and renormalization scale dependence, at small p_T's, similarly to what has been observed in photon–hadron and hadron–hadron collisions. In this region, the contribution of the resolved channels is sizeable, and the theoretical predictions are mildly dependent upon the choice of the photonic parton densities. However, this dependence is smaller than that due to mass or renormalization scale choice, and this prevents a discrimination of the different density sets, even in the ideal case in which the charm mass would be known exactly. As far as the comparison with the data available at present is concerned, we find a good agreement in the shape of the p_T and η distributions, and a reasonable agreement as far as the absolute normalization is concerned. In general, the comparison between NLO QCD and the experimental results reproduces the pattern already known from other types of collisions; namely, theory somewhat underestimates the data, and a special tuning of the input parameters is needed to improve the agreement. The mild dependence of the theoretical predictions for the visible cross section upon the input parameters appears to imply that it will be difficult to constrain any of these parameters by comparing theory with data. On the other hand, when the statistical significance of the measurements will be increased, charm production in photon–photon collisions will be a valuable tool in testing the underlying production dynamics.

Acknowledgements

We would like to thank Jochen Patt and Stefan Söldner-Rembold for their enthusiastic encouragement and for providing us with the OPAL data. We are grateful to Valeri An-

dreev, Alex Finch, Albert de Roeck, Gueorgui Soultanov and Andreas Vogt for valuable discussions. The work of S.F. and M.K. is supported in part by the EU Fourth Framework Programme 'Training and Mobility of Researchers', Network 'Quantum Chromodynamics and the Deep Structure of Elementary Particles', contract FMRX-CT98-0194 (DG 12 - MIHT). The work of E.L. is part of the research program of the Foundation for Fundamental Research of Matter (FOM) and the National Organization for Scientific Research (NWO).

APPENDIX: PHOTON–PHOTON CROSS SECTIONS

In this appendix we describe some technical aspects of the computation of charm cross sections in photon–photon collisions. In particular, we will discuss in some detail the issue of scheme dependence of the direct and resolved production mechanisms.

We consider the process

$$e^+ + e^- \quad \longrightarrow \quad e^+ + e^- + \underbrace{\gamma + \gamma}_{\hookrightarrow Q + \overline{Q}}. \tag{4}$$

The final-state positron and electron are scattered almost collinearly to the beam line; thus, the photons eventually producing the heavy quark pair are (almost) on-shell. The cross section can therefore be written as follows

$$d\sigma_{ee}(P_{e^+}, P_{e^-}) = \int dx_{e^+} dx_{e^-} f_\gamma^{(e)}(x_{e^+}) f_\gamma^{(e)}(x_{e^-}) d\hat{\sigma}(x_{e^+} P_{e^+}, x_{e^-} P_{e^-}), \tag{5}$$

where $d\hat{\sigma}$ is the cross section for the process $\gamma\gamma \to Q\bar{Q}$, and $f_\gamma^{(e)}$ is the Weizsäcker–Williams function [15]. We introduce the short-hand notation

$$d\sigma_{ee} = f_\gamma^{(e)} * d\hat{\sigma} * f_\gamma^{(e)}, \tag{6}$$

which defines the $*$ symbol. As mentioned in section 2, three mechanisms contribute to the two-photon cross section:

$$d\hat{\sigma} = d\hat{\sigma}_{\gamma\gamma} + d\hat{\sigma}_{1r} + d\hat{\sigma}_{2r}, \tag{7}$$

where the three terms in the RHS of this equation denote the direct, single-resolved, and double-resolved components, respectively. Using the factorization theorems in QCD, the single- and double-resolved cross sections can be written as the convolution of the partonic hard-scattering cross sections $d\hat{\sigma}_{i\gamma}$, $d\hat{\sigma}_{\gamma i}$ and $d\hat{\sigma}_{ij}$ with the parton densities in the photon $f_i^{(\gamma)}$:

$$d\hat{\sigma}_{1r} = f_i^{(\gamma)} * d\hat{\sigma}_{i\gamma} + d\hat{\sigma}_{\gamma i} * f_i^{(\gamma)}, \tag{8}$$

$$d\hat{\sigma}_{2r} = f_i^{(\gamma)} * d\hat{\sigma}_{ij} * f_j^{(\gamma)}, \tag{9}$$

Here, a summation over repeated indices is understood, and the indices i, j run over all the parton flavours $u, \bar{u}, \cdots, g$. We can summarize the content of eqs. (7), (8) and (9) by writing

$$d\hat{\sigma} = F_a^{(\gamma)} * d\hat{\sigma}_{ab} * F_b^{(\gamma)}, \tag{10}$$

	Direct	Single-res.	Double-res.
$2 \to 2$	$\gamma\gamma \to Q\overline{Q}$	$\gamma g \to Q\overline{Q}$	$gg \to Q\overline{Q}$
			$q\bar{q} \to Q\overline{Q}$
$2 \to 3$	$\gamma\gamma \to Q\overline{Q}g$	$\gamma g \to Q\overline{Q}g$	$gg \to Q\overline{Q}g$
		$\gamma q \to Q\overline{Q}q$	$q\bar{q} \to Q\overline{Q}g$
			$qg \to Q\overline{Q}q$

Table 2: *Partonic subprocesses contributing to heavy-quark production in $\gamma\gamma$ collisions at next-to-leading order.*

where the indices a and b run over all parton flavours, plus the photon. The generalized densities in the photon are given by

$$F_a^{(\gamma)}(x) = \delta_{a\gamma}\delta(1-x) + f_a^{(\gamma)}(x)\,(1-\delta_{a\gamma})\,. \tag{11}$$

The three quantities on the RHS of eq. (7) are separately divergent order by order in perturbation theory, and scheme-dependent. The only quantity that is finite and scheme-independent at all orders is $d\hat{\sigma}$. However, as mentioned in the introduction, the reaction we study has the special feature that the scheme dependence of the direct component and of the sum of the resolved components only starts beyond NLO. Although that still does not make these cross sections physically observable, it does give us a fairly clear idea of how often the initial photon fluctuates to a hadronic state at the energies considered. Let us therefore clarify the issue of scheme dependence by working out the specifics in some detail. We write the perturbative expansions of the partonic cross sections as:

$$d\hat{\sigma}_{\gamma\gamma} = \alpha_{\rm em}^2 \sum_{n=0}^{\infty} \alpha_S^n d\hat{\sigma}_{\gamma\gamma}^{(n)}, \tag{12}$$

$$d\hat{\sigma}_{i\gamma} = \alpha_{\rm em}\alpha_S \sum_{n=0}^{\infty} \alpha_S^n d\hat{\sigma}_{i\gamma}^{(n)}, \tag{13}$$

$$d\hat{\sigma}_{ij} = \alpha_S^2 \sum_{n=0}^{\infty} \alpha_S^n d\hat{\sigma}_{ij}^{(n)}. \tag{14}$$

The expansion of $d\hat{\sigma}_{\gamma i}$ is identical to that of $d\hat{\sigma}_{i\gamma}$ in eq. (13). In what follows, we restrict ourselves to the first non-trivial QCD corrections (which amounts to retaining the first two terms in the sums of eqs. (12)–(14)); this is phenomenologically relevant, since no complete NNLO result is available for heavy-flavour production. At this order, only (tree-level and loop) $2 \to 2$ and (tree-level) $2 \to 3$ partonic processes contribute to the result; they are listed in table 2 for the three production channels.

A general two-photon cross section such as $d\hat{\sigma}$, being a physical observable, must be

scheme-independent. Therefore, an expression equivalent to eq. (10) is

$$d\hat{\sigma} = F_a^{(\gamma)'} * d\hat{\sigma}'_{ab} * F_b^{(\gamma)'}, \tag{15}$$

where the prime denotes that the generalized densities and the partonic cross sections, which are non-physical, are calculated in a scheme different from that used in eq. (10). In QCD, the parton densities expressed in two different schemes can always be related as follows:

$$F_a^{(\gamma)'} = \delta_{a\gamma}\delta + f_a^{(\gamma)'}\left(1-\delta_{a\gamma}\right), \quad f_i^{(\gamma)'} = f_i^{(\gamma)} + \alpha_{\rm em}H_i + \alpha_S K_{ij}\otimes f_j^{(\gamma)}, \tag{16}$$

where H_i and K_{ij} are functions and distributions, respectively, with an expansion in α_S starting from α_S^0. The symbol $\otimes$ denotes the convolution integral

$$A\otimes B(z) = B\otimes A(z) = \int dxdy\,\delta(z-xy)\,A(x)B(z). \tag{17}$$

Substituting eq. (16) into eq. (15), and using eqs. (12)–(14) we find:

$$\begin{aligned}
d\hat{\sigma} &= \alpha_{\rm em}^2 d\hat{\sigma}_{\gamma\gamma}^{(0)'} + \alpha_{\rm em}^2\alpha_S\left[d\hat{\sigma}_{\gamma\gamma}^{(1)'} + H_i * d\hat{\sigma}_{i\gamma}^{(0)'} + d\hat{\sigma}_{\gamma i}^{(0)'} * H_i\right] \\
&+ \alpha_{\rm em}\alpha_S\left[f_i^{(\gamma)} * d\hat{\sigma}_{i\gamma}^{(0)'} + d\hat{\sigma}_{\gamma i}^{(0)'} * f_i^{(\gamma)}\right] + \alpha_{\rm em}\alpha_S^2\left[f_i^{(\gamma)} * d\hat{\sigma}_{i\gamma}^{(1)'} + d\hat{\sigma}_{\gamma i}^{(1)'} * f_i^{(\gamma)}\right. \\
&+ \left.\left(K_{ik}\otimes f_k^{(\gamma)}\right) * d\hat{\sigma}_{i\gamma}^{(0)'} + d\hat{\sigma}_{\gamma i}^{(0)'} * \left(K_{ik}\otimes f_k^{(\gamma)}\right) + H_i * d\hat{\sigma}_{ij}^{(0)'} * f_j^{(\gamma)} + f_i^{(\gamma)} * d\hat{\sigma}_{ij}^{(0)'} * H_j\right] \\
&+ \alpha_S^2 f_i^{(\gamma)} * d\hat{\sigma}_{ij}^{(0)'} * f_j^{(\gamma)} + \alpha_S^3\left[f_i^{(\gamma)} * d\hat{\sigma}_{ij}^{(1)'} * f_j^{(\gamma)} + f_i^{(\gamma)} * d\hat{\sigma}_{ij}^{(0)'} * \left(K_{jk}\otimes f_k^{(\gamma)}\right)\right. \\
&+ \left.\left(K_{ik}\otimes f_k^{(\gamma)}\right) * d\hat{\sigma}_{ij}^{(0)'} * f_j^{(\gamma)}\right] + \mathcal{O}\left(\alpha_{\rm em}^2\alpha_S^2, \alpha_{\rm em}\alpha_S^3, \alpha_S^4\right).
\end{aligned} \tag{18}$$

Using only the first term in the expansion in α_S of H_i and K_{ij} (which we denote as $H_i^{(0)}$ and $K_{ij}^{(0)}$, respectively), and comparing eq. (18) with eq. (7), we get

$$d\hat{\sigma}_{\gamma\gamma}^{(0)'} = d\hat{\sigma}_{\gamma\gamma}^{(0)}, \quad d\hat{\sigma}_{i\gamma}^{(0)'} = d\hat{\sigma}_{i\gamma}^{(0)}, \quad d\hat{\sigma}_{\gamma i}^{(0)'} = d\hat{\sigma}_{\gamma i}^{(0)}, \quad d\hat{\sigma}_{ij}^{(0)'} = d\hat{\sigma}_{ij}^{(0)}, \tag{19}$$

$$d\hat{\sigma}_{\gamma\gamma}^{(1)'} = d\hat{\sigma}_{\gamma\gamma}^{(1)} - H_i^{(0)} * d\hat{\sigma}_{i\gamma}^{(0)} - d\hat{\sigma}_{\gamma i}^{(0)} * H_i^{(0)}, \tag{20}$$

$$d\hat{\sigma}_{i\gamma}^{(1)'} = d\hat{\sigma}_{i\gamma}^{(1)} - K_{ki}^{(0)} * d\hat{\sigma}_{k\gamma}^{(0)} - d\hat{\sigma}_{ik}^{(0)} * H_k^{(0)}, \tag{21}$$

$$d\hat{\sigma}_{\gamma i}^{(1)'} = d\hat{\sigma}_{\gamma i}^{(1)} - d\hat{\sigma}_{\gamma k}^{(0)} * K_{ki}^{(0)} - H_k^{(0)} * d\hat{\sigma}_{ki}^{(0)}, \tag{22}$$

$$d\hat{\sigma}_{ij}^{(1)'} = d\hat{\sigma}_{ij}^{(1)} - d\hat{\sigma}_{ik}^{(0)} * K_{kj}^{(0)} - K_{ki}^{(0)} * d\hat{\sigma}_{kj}^{(0)}, \tag{23}$$

where use has been made of the fact that

$$(A\otimes B) * C = A * (B * C). \tag{24}$$

Equation. (19) is nothing but the formal statement that, at leading order, the cross sections are independent of the scheme adopted. This equation also implies that, *at this order*, the direct, single-resolved, and double-resolved terms are separately physically meaningful. The inclusion of radiative corrections, however, changes the situation, as can be clearly seen from eqs. (20)–(23). For instance, when changing the scheme, the single-resolved cross section (eqs. (21) and (22)) receives a contribution from the double-resolved part. In principle, this is also true for the direct cross section (eq. (20)). Note, however, that for heavy flavour

production, if i is a gluon, then $H_i^{(0)}$ is zero, while if i is a quark, then $d\hat{\sigma}_{i\gamma}^{(0)}$ is zero (this is not true for – say – jet production, where $d\hat{\sigma}_{q\gamma}^{(0)}$ is non-vanishing). Therefore, at next-to-leading order the direct term is scheme-independent, while the single- and double-resolved terms are closely related, since one is entitled to add to them a finite piece without changing their sum. Clearly, when going to next-to-next-to-leading order, the direct cross section will also become scheme-dependent.

References

[1] For a recent review, see for example: S. Frixione, M.L. Mangano, P. Nason and G. Ridolfi, in *Heavy Flavours II*, eds. A.J. Buras and M. Lindner (World Scientific, Singapore, 1998) [hep-ph/9702287].

[2] J. Patt, for the OPAL Collaboration, *Photon 99*, 23-27 May 1999, Freiburg im Breisgau, Germany.

[3] L3 Collaboration, submitted to the *International Europhysics Conference High Energy Physics 99*, 15-21 July 1999, Tampere, Finland; CERN preprint CERN-EP/99-106.

[4] M.L. Mangano, P. Nason and G. Ridolfi, Nucl. Phys. **B373** (1992) 295 [hep-ph/9306337].

[5] S. Frixione, M.L. Mangano, P. Nason and G. Ridolfi, Nucl. Phys. **B412** (1994) 225 [hep-ph/9306337].

[6] M. Krämer and E. Laenen, Phys. Lett. **B371** (1996) 303 [hep-ph/9511358].

[7] M. Drees, M. Krämer, J. Zunft and P.M. Zerwas, Phys. Lett. **B306** (1993) 371.

[8] M. Glück, E. Reya and A. Vogt, Phys. Rev. **D46** (1992) 1973.

[9] P. Aurenche, J.P. Guillet and M. Fontannaz, Z. Phys. **C64** (1994) 621 [hep-ph/9406382].

[10] L.E. Gordon and J.K. Storrow, Nucl. Phys. **B489** (1997) 405 [hep-ph/9607370].

[11] M. Glück, E. Reya and I. Schienbein, Phys. Rev. **D60** (1999) 054019 [hep-ph/9903337].

[12] M. Cacciari and M. Greco, Phys. Rev. **D55** (1997) 7134 [hep-ph/9702389].

[13] J. Binnewies, B.A. Kniehl and G. Kramer, Phys. Rev. **D58** (1998) 014014 [hep-ph/9712482].

[14] P. Nason and C. Oleari, preprint BICOCCA-FT-99-07 [hep-ph/9903541].

[15] C.F. Weizsäcker, Z. Phys. **88** (1934) 612; E.J. Williams, Phys. Rev. **45** (1934) 729.

[16] P. Nason, S. Dawson and R.K. Ellis, Nucl. Phys. **B327** (1989) 49 (Erratum: *ibid.* **B335** (1990) 260).

[17] R.K. Ellis and P. Nason, Nucl. Phys. **B312** (1989) 551.

[18] M. Glück, E. Reya and A. Vogt, Phys. Rev. **D45** (1992) 3986.

[19] S. Frixione, M.L. Mangano, P. Nason and G. Ridolfi, Phys. Lett. **B319** (1993) 339 [hep-ph/9310350].

[20] C. Peterson, D. Schlatter, I. Schmitt and P. Zerwas, Phys. Rev. **D27** (1983) 105.

[21] A. Vogt, talk given at *Photon 99*, 23-27 May 1999, Freiburg im Breisgau, Germany [hep-ph/9908315]; Phys. Lett. **B354** (1995) 145 [hep-ph/9504285].

[22] B. Mele and P. Nason, Nucl. Phys. **B361** (1991) 626.

[23] M. Cacciari, M. Greco, B.A. Kniehl, M. Krämer, G. Kramer and M. Spira, Nucl. Phys. **B466** (1996) 173 [hep-ph/9512246].

[24] M. Cacciari, M. Greco and P. Nason, JHEP **05** (1998) 007 [hep-ph/9803400].

[25] J. Chrin, Z. Phys. **C36** (1987) 163.